RSC Advances

PAPER

View Article Online
View Journal | View Issue

Cite this: *RSC Adv.*, 2024, **14**, 5045

Anti-cancer activity of zinc-tetraphenylporphyrin photosensitizer/dextran-*graft*-polyacrylamide copolymer/Au(Ag) nanoparticle nanohybrids†

Oleg Yeshchenko,[a] Nataliya Kutsevol,[b] Pavlo Virych, *[b] Pavlo Khort,[a] Petro Virych,[c] Vasyl Chumachenko[b] and Vasyl Cekhun[c]

A comparative study of *in vitro* anti-cancer photodynamic activities of three-component zinc-tetraphenylporphyrin photosensitizer/dextran-*graft*-polyacrylamide copolymer/Au(Ag) nanoparticle (ZnTPP/D-*g*-PAA/Au(Ag)NP) nanohybrids on LNCaP prostate cancer cells was carried out under 420 nm light irradiation with low power. A significant cytotoxic effect was revealed for both ZnTPP/D-*g*-PAA/AgNP and ZnTPP/D-*g*-PAA/AuNP nanohybrids, where ZnTPP/D-*g*-PAA/AgNP nanohybrids exhibited considerably higher anticancer activity (82%) compared to ZnTPP/D-*g*-PAA/AuNP nanohybrids (45%). The higher activity of silver-containing nanohybrids is rationalized based on two factors. The first factor is the resonance of 420 nm light with a absorption Soret peak of the ZnTPP photosensitizer and a localized surface plasmon mode in Ag nanoparticles. Correspondingly, the plasmon enhancement of reactive oxygen species photogeneration by ZnTPP molecules was considerably higher for the nanohybrid containing silver compared to the one containing gold. The second factor is the higher cytotoxicity of Ag nanoparticles compared to Au ones. The study results prove the high potential of D-*g*-PAA/Ag(Au)NP nanohybrids combined with 420 nm light irradiation with low power in the photodynamic treatment of prostate cancer.

Received 15th November 2023
Accepted 23rd January 2024

DOI: 10.1039/d3ra07825f

rsc.li/rsc-advances

Introduction

Photodynamic therapy (PDT) is a modern, non-invasive, rapidly developing, and promising therapeutic approach for a wide range of cancers.[1–4] PDT is based on the interaction between light and photosensitive compounds, leading to the generation of cytotoxic reactive oxygen species (ROS). Under appropriate light irradiation, non-toxic photosensitizer (PS) molecules are activated, entering an excited electronic state, thus becoming effective electron donors. Oxygen molecules play the role of electron acceptors, resulting in ROS generation. ROS irreversibly damage tumor cells, thereby causing cell death *via* necrosis or apoptosis.[5–7] However, for the effective application of PDT, it is necessary to overcome some disadvantages associated with the limited solubility of PS molecules in water. Water causes aggregation of PS molecules and subsequent reduction of singlet-oxygen photogeneration. In this respect, to increase PDT efficacy, nanotechnology methods can be used to modify existing photosensitizers and provide the target delivery of drugs to tumor cells.[8,9] A promising direction for the treatment of malignant tumors is the use of complex nanomaterials, which include several components with special functions, potentially enhancing their therapeutic effect.[10–15] In particular, such complex nanomaterials are hybrid nanosystems containing photosensitizers, metal nanoparticles (NPs) and polymers.

The significant potential for utilizing noble metal NPs in cancer treatment also lies in the application of localized surface plasmon resonance (LSPR). This is primarily owing to the phenomenon of plasmon enhancement. The excitation of LSPR in metal NPs strengthens the local electric field near the NP surface. This intensified local electric field enhances optical processes in molecules functionalized on the surface of metal NPs or near the rough metal surface, such as surface-enhanced Raman scattering (SERS), surface-enhanced absorption (SEA), surface-enhanced fluorescence (SEF) and photocatalysis.[16–19] The plasmon-enhanced light absorption by PS molecules near the metal NP surface in hybrid nanosystems (nanohybrids) leads to more efficient ROS generation (singlet oxygen in particular), consequently augmenting PDT efficiency.[20–25] A scheme demonstrating the idea of the plasmonic enhancement of the photogeneration of singlet oxygen in a three-component (PS/polymer/metal NPs) hybrid nanosystem is discussed in this study (Fig. 1). Gold (Au) NPs possess distinctive physical and

[a]*Faculty of Physics, Taras Shevchenko National University of Kyiv, 60 Volodymyrska Str., 01601 Kyiv, Ukraine*

[b]*Faculty of Chemistry, Taras Shevchenko National University of Kyiv, 60 Volodymyrska Str., 01601 Kyiv, Ukraine. E-mail: pavlo.virych@knu.ua*

[c]*R.E. Kavetsky Institute for Experimental Pathology, Oncology and Radiobiology, 45 Vasylkivska Str., 03022, Kyiv, Ukraine*

† Electronic supplementary information (ESI) available. See DOI: https://doi.org/10.1039/d3ra07825f.

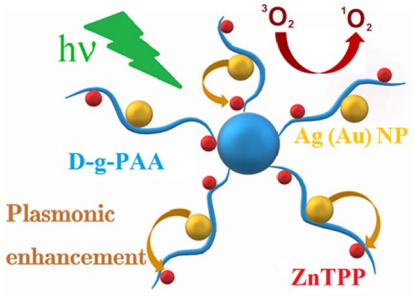

Fig. 1 Scheme demonstrating the idea of the plasmonic enhancement of photogeneration of singlet oxygen in the studied ZnTPP/D-*g*-PAA/Ag(Au)NP hybrid nanosystem.

chemical properties, primarily including low toxicity, stability, easy synthesis, small size, plasmonic effects, and high permeability into the tissue. These attributes enable their application in medicine for diagnostic purposes and for the treatment of various diseases, particularly cancer.[26,27] Conversely, silver (Ag) NPs have demonstrated antitumor activity, with apoptosis being the predominant mode of cell death. Studies have indicated the initiation of DNA damage in cancer cells because of ROS generation, as evidenced by alterations in mitochondrial membrane potential.[28]

Polymeric nanomaterials are at the forefront of biomedical research. The use of biocompatible, water-soluble polymers in nanomedicine can enhance the bioavailability and pharmacokinetics of therapeutic agents, thereby improving their effectiveness.[29] Polymers can serve as an effective matrix for the synthesis of metal NPs, preventing their aggregation and facilitating size regulation.[30] The multifunctionality of polymeric molecules, with their unique chemical and biological properties, enables the superior delivery and controlled release of various therapeutic agents.[31–35] Encapsulation of PS in a polymer matrix prevents the aggregation of hydrophobic dye molecules, significantly improving PDT efficiency in biological environments.[36] Recently, the dextran-*graft*-polyacrylamide copolymer (D-*g*-PAA) used in this study has been demonstrated to be an effective nanocarrier for photosensitizers, Au and AgNPs, as well as anticancer drugs, such as cisplatin and doxorubicin.[37]

Currently, the most effective photosensitizers (PSs) used in photodynamic therapy (PDT), including treatments for cancer and bacterial infections, are based on porphyrin and its derivatives.[37] Porphyrins have several advantages as photosensitizers, including stability, efficient absorption of visible light, high yield of ROS photogeneration, easy functional modification, long triplet state lifetime, and low dark toxicity. Metalloporphyrins have attracted considerable interest in recent years. To stabilize the porphyrin ring and preserve the photophysical properties of PS, zinc can be integrated into the porphyrin ring. These structures, such as zinc-tetraphenylporphyrin (ZnTPP), more closely resemble natural porphyrins compared to *meso*-substituted porphyrins and are extensively used in biological research. Some studies have reported that the presence of zinc in the porphyrin ring reduces mitochondrial binding and encourages membrane binding due to the formation of complexes with phospholipid phosphate groups, thereby enhancing the photodynamic effect.[38]

In this study, we conducted comparative studies of the anticancer activity of triple nanohybrids consisting of zinc-tetraphenylporphyrin (ZnTPP) photosensitizer, dextran-*graft*-polyacrylamide (D-*g*-PAA) copolymer, and Au(Ag) nanoparticles based on the presence of either Au or Ag nanoparticles in the nanosystem. The PDT activity of the investigated nanohybrids was found to be significantly high, demonstrating their considerable potential in anticancer PDT therapy. The identified characteristics of the anticancer PDT activity of these nanohybrids are in good agreement with their antibacterial PDT activity, as reported in our recent studies.[39–41]

Experimental

Synthesis of nanohybrids

All chemicals utilized for the synthesis of hybrid nanosystems, excluding acrylamide, were sourced from Merck and were used without additional purification. The star-like copolymer dextran-*graft*-polyacrylamide (D-*g*-PAA) was used as a matrix for the *in situ* preparation of nanosystems. The synthesis and characterization of D-*g*-PAA have been reported elsewhere.[42] This copolymer has proven effective as a nanocarrier of drugs for chemotherapy and photodynamic therapy.[36,43,44]

Nanosystem preparation

D-*g*-PAA stock solution. 1 g of D-*g*-PAA was dissolved in 100 mL of deionized water and left for 24 hours to ensure complete dissolution.

D-*g*-PAA/AuNPs. 0.1 mL of aqueous $HAuCl_4$ (10^{-2} M) was added to 0.9 mL of the D-*g*-PAA stock solution. After 20 minutes of stirring, 0.04 mL of a freshly prepared $NaBH_4$ solution (10^{-1} M) was added at once, and the mixture was stirred for an additional 20 minutes. A change in the ruby-red color indicated the formation of Au NPs.

D-*g*-PAA/AgNPs. 0.1 mL of aqueous $AgNO_3$ (10^{-2} M) was added to 0.9 mL of the D-*g*-PAA stock solution. After 20 minutes of stirring, 0.04 mL of a freshly prepared $NaBH_4$ solution (10^{-1} M) was added all at once, and the mixture was stirred for another 20 minutes. The solution turned orange in color, indicating the formation of Ag NPs.

ZnTPP/D-*g*-PAA/Au(Ag)NPs. Zinc tetraphenylporphyrin (ZnTPP) was used as a photosensitizer (PS). The appropriate volume of ZnTPP (10^{-3} g mL^{-1}) solution in DMSO was added to the D-*g*-PAA/AuNPs or D-*g*-PAA/$AgNO_3$ stock solution and stirred for 20 minutes.

Because the ZnTPP photosensitizer is hydrophobic, when it is added to aqueous solutions of D-*g*-PAA and D-*g*-PAA/AgNPs, ZnTPP molecules tend to form aggregates. In this regard, the concentration of ZnTPP in aqueous solutions cannot be large. However, at very low concentrations in which aggregate formation is absent, the photosensitizer has almost no biological activity. Based on these considerations, in our recent works,[39–41] an intermediate concentration of ZnTPP (0.001 mg mL^{-1}) was

experimentally determined for aqueous solutions of nanohybrids containing polymers, metal nanoparticles and ZnTPP. At this concentration, there was no significant aggregation, but the nanohybrids already showed pronounced antibacterial biological PDT activity. Therefore, in the present work, a concentration of 0.001 mg mL^{-1} was used in all studies.

FTIR spectroscopy

FTIR spectra for D-*g*-PAA were obtained on a Nicolet NEXUS-475 FTIR spectrophotometer (GMI) in the range of 4000–400 cm^{-1} using thin (6–9 μm) polymer films. The films were created from aqueous solutions.

Morphology and size characterization: TEM and DLS

Transmission electron microscopy (TEM) was performed on the samples using a CM12 microscope (FEI). TEM images were obtained using a Megaview SIS camera. However, D-*g*-PAA macromolecules, ZnTPP molecules, and aggregates exhibit significantly lower contrast compared to metal NPs, making them invisible in TEM images. Therefore, dynamic light scattering (DLS) was used to gather information about the size and morphological characteristics of the investigated nanosystems. The hydrodynamic particle size distribution (PSD) for the nanosystems in water was measured using a NanoBrook Omni particle size analyzer (Brookhaven) equipped with a 532 nm laser. The scattered light was recorded in the backscattering geometry at an angle of 173°. The PSD was obtained from the autocorrelation functions calculated using the non-negative truncated singular decomposition method.[45] DLS measurements were conducted at a room temperature of 20 °C, two hours after mixing the ZnTPP–ethanol solution with water or aqueous solutions of D-*g*-PAA and D-*g*-PAA/AuNPs.

Optical spectroscopy

Absorption spectra were measured using a Cary 60 ultraviolet-visible (UV-vis) spectrophotometer (Agilent). Fluorescence (FL) spectra were measured using a Shimadzu RF-6000 spectrofluorophotometer (Shimadzu) with an excitation wavelength of 420 nm. The 420 nm wavelength was used for FL excitation because it coincides spectrally with the most intensive B peak of the absorption spectrum of the ZnTPP photosensitizer. Samples of the solutions were placed in 1 cm × 4 cm quartz cell. Measurements of absorption and FL spectra were performed 2 hours after mixing the ZnTPP–ethanol solution with water, aqueous solutions of D-*g*-PAA and D-*g*-PAA/AuNPs, following the completion of transient processes of penetration of ZnTPP molecules into D-*g*-PAA and D-*g*-PAA/AuNP macromolecules and binding to them. The FL anisotropy was determined as $r = \frac{I_{VV} - GI_{VH}}{I_{VV} + 2GI_{VH}}$, where I_{ij} is the FL intensity, the *ij* indices denote the orientation of the polarizers before and after the sample, respectively (V – vertical; H – horizontal), and $G = I_{HV}/I_{HH}$ is the lattice factor.

Anticancer activity *in vitro*

The study was conducted using the prostate cancer cell line LNCaP, sourced from the cell line bank of the R.E. Kavetsky Institute of Experimental Pathology, Oncology, and Radiobiology of the National Academy of Sciences of Ukraine. Cells were cultured in a complete nutrient Dulbecco's Modified Eagle Medium (DMEM) (Cat 11995065, Thermo Fisher) with elevated glucose and pyruvate concentrations, 10% newborn calf serum (NCS), 40 μg per mL gentamicin, with a 5% CO_2 atmosphere at 37 °C. Nanohybrid solutions were added to the incubation medium using a two-fold dilution method in the concentration range of 0.172–0.001 mg mL^{-1} and incubated for 48 hours at 37 °C.

The cytotoxicities of the D-*g*-PAA copolymer as well as gold and silver NPs were assessed using a two-fold dilution method from an initial concentration of 0.172 mg mL^{-1} for Au NPs and 0.023 mg mL^{-1} for Ag NPs. Phototoxicity at 420 nm light was determined across a range of irradiation doses of 1–5 J cm^{-2} with a light power of 5, 10, and 20 mJ s^{-1}. The irradiation dose for LNCaP cells with nanohybrids was set at 1 and 2 J cm^{-2} with a light power of 10 mJ s^{-1}. A 420 nm light was selected for irradiation because it coincides spectrally with the most intensive B peak of the absorption spectrum of the ZnTPP photosensitizer. The number of viable cells was calculated photometrically after staining with crystal violet. The medium was removed, and 50 μL of a crystal violet solution (5 mg per mL dye in 70% methyl alcohol) was added to each well. After 10 minutes, the dye was rinsed off three times with water. Results were recorded using a multiwell spectrophotometer at an excitation wavelength of 540 nm. The percentage of cell viability inhibition was calculated as follows: $IR = (1 - D_{exp}/D_{contr}) \times 100$, where IR is the cytotoxicity given in %, D_{exp} is the optical density of experimental well at 540 nm, and D_{contr} is the optical density of control well at 540 nm.

ROS detection

Prostate cancer LNCaP cells were used. The cells were incubated in DMEM (BioWest, France) with elevated glucose and pyruvate concentrations, 10% fetal bovine serum (BioWest) and 100 U per mL penicillin/streptomycin (Thermo Fisher Scientific, USA) at 37 °C, and 5% CO_2. 3×10^5 cells were seeded. The cells were incubated for 2 h with the ZnTPP/D-*g*-PAA (0.001 mg mL^{-1}), D-*g*-PAA/AgNPs (0.0047 mg mL^{-1}), and D-*g*-PAA/AuNPs (0.086 mg mL^{-1}). The cells were irradiated at 420 nm. The light power was 10 mJ s^{-1}, and the irradiation doses were 1 J cm^{-2} and 2 J cm^{-1}.

To detect ROS level, cells were resuspended in 0.5 mL of 15 μM 2′,7′-dichlorofluorescein diacetate (Sigma-Aldrich, USA) and incubated for 40 minutes at 37 °C. The cells were washed with 1.5 mL of phosphate saline buffer (PBS, Biowest) and centrifuged at 400 g for 10 min. The cells were resuspended in 0.5 mL of PBS and analyzed using a flow cytometer (DxFlex, Beckman Coulter, Brea, California, USA). Fluorescence intensity was analyzed using the FITC channel (light filter 525/40 nm).

At least 10 000 life cells were analyzed for each sample. Primary data processing was carried out using CytExpert software. The studies were repeated three times.

Statistical analysis

Mathematical and statistical processing of the obtained results was carried out using one-factor ANOVA analysis, Scheffe's test

or Kruskal–Wallis test for non-parametric data ($p < 0.05$). Results were presented as mean and standard deviation ($M \pm$ SD).

Results and discussion

FTIR characterization

The FTIR spectrum of the D-*g*-PAA shows the characteristic peaks of PAA ranging from 3150 to 3250 cm^{-1} (stretching of –OH/NH_2 of PAA) and 2900 to 2950 cm^{-1} (symmetric and asymmetric stretching of $–CH_2$ of PAA), but it is not reasonable to analyze this region of spectra because of the presence of water in the sample with strong characteristic –OH stretching bands, which overlap with the bands of the polymer. Two strong bands at 1650–1660 cm^{-1} and 1615 cm^{-1} corresponding to amide 1 (C═O stretching) and amide 2 (N–H bending), respectively, are characteristic bands of PAA.[46] The amount of dextran component (about 4%) is so low that it can be negligible. FTIR spectra are shown in ESI Fig. S1.†

Morphology and size characterization of nanohybrids

TEM. The typical TEM images of D-*g*-PAA/AuNPs and D-*g*-PAA/AgNPs nanohybrids are presented in Fig. 2. The Au NPs exhibit a spherical shape with an average size (diameter) of 5.0 nm (Fig. 2(a) and (b)). Similarly, the Ag NPs are also spherical and have an average size of 7.2 nm. The polymer component, D-*g*-PAA, is not discernible in the TEM images owing to the significantly lower contrast compared to the metal NPs. However, it can be observed that both Au and Ag NPs are predominantly grouped together, indicating their binding to D-*g*-PAA macromolecules, although some metal NPs remain unbound. Moreover, the ZnTPP molecules are not visible in the TEM images due to their small size and low contrast.

Dynamic light scattering. Because the TEM method does not allow the determination of the sizes of components, such as polymer and photosensitizer, in the nanohybrid, we also used the DLS method. The resulting PSD (particle hydrodynamic size distribution) for aqueous solutions of D-*g*-PAA polymer, as well as ZnTPP/D-*g*-PAA/AuNP and ZnTPP/D-*g*-PAA/AgNP nanohybrids, is illustrated in Fig. 3. Given that nanohybrids in water can potentially be unstable, DLS measurements were taken both 1 hour and 24 hours after the nanohybrids were prepared (by adding ZnTPP to D-*g*-PAA/AuNP and D-*g*-PAA/AgNP solutions). We found that ZnTPP/D-*g*-PAA/AuNP and ZnTPP/D-*g*-PAA/AgNP nanohybrids in water are both aggregatively and sedimentationally stable, as indicated by the consistent PSD.

The PSD for the D-*g*-PAA polymer displays a single peak corresponding to a hydrodynamic diameter (D_H) of 78 nm (Fig. 3, black line). The ZnTPP/D-*g*-PAA/AuNP nanohybrid is characterized by two PSD peaks at 4.2 nm and 84 nm (Fig. 3, red line). The first peak at 4 nm is attributed to Au NPs, and the second one corresponds to ZnTPP/D-*g*-PAA/AuNP hybrid macromolecules. The PSD of The ZnTPP/D-*g*-PAA/AgNP nanohybrid also contains two peaks at 4.9 nm and 79 nm (Fig. 3, blue line). The first peak at 4.9 nm corresponds to Ag NPs, while the second one corresponds to ZnTPP/D-*g*-PAA/AgNP hybrid macromolecules. The data indicate that the incorporation of ZnTPP molecules and Au and Ag NPs has a minimal impact on the size of the polymer macromolecule, suggesting the absence of aggregates of ZnTPP and metal NPs within the hybrid macromolecules. It is also noteworthy that a close agreement between the average sizes of Au and Ag NPs is determined by TEM (5 nm and 7 nm, respectively) and DLS (4 nm and 5 nm, respectively). Despite the low intensity of the PSD peaks

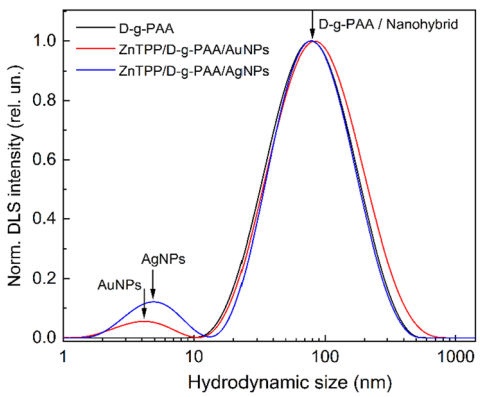

Fig. 3 DLS size distribution of D-*g*-PAA, ZnTPP/D-*g*-PAA/AuNP and ZnTPP/D-*g*-PAA/AgNP aqueous solution.

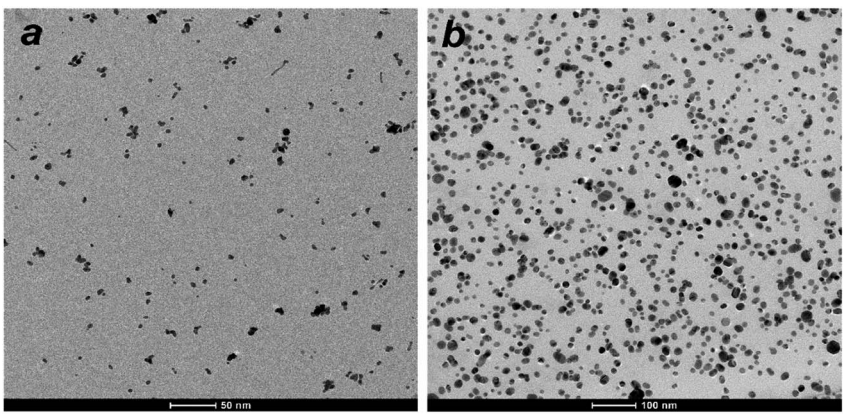

Fig. 2 TEM images of D-*g*-PAA/AuNPs (a) and D-*g*-PAA/AgNP (b) nanohybrids.

for Au and Ag NPs, the concentration of metal NPs in the studied solutions is quite substantial. This is because the intensity of Rayleigh scattering of light by small particles depends on their size as D_H^6.

Light absorption and fluorescence

The nanohybrids of ZnTPP/D-*g*-PAA/AuNPs and ZnTPP/D-*g*-PAA/AgNPs were characterized by absorption and fluorescence (FL) spectroscopies (Fig. 4 and 5, respectively). For reference, the absorption spectrum of the ZnTPP photosensitizer in ethanol was also measured (Fig. 4 and 5, black line). The absorption spectrum of ZnTPP in ethanol exhibits a typical structure of porphyrins in organic solvents.[47–50] Specifically, it contains an intense B (Soret) peak with a characteristic doublet structure in the range of 385–440 nm, maximum at 420 nm, and a group of low-intensity Q peaks in the range of 530–620 nm. The Q and B peaks originate from the absorptive transitions from the electron ground state to the 1st and 2nd excited electronic states of the porphyrin molecule, respectively. Similarly, the FL spectrum of ZnTPP in ethanol exhibits a doublet structure, similar to those of other porphyrins, featuring short-wavelength (602 nm) F_{00} and long-wavelength (655 nm) F_{01} peaks.[20,35] These peaks originate from the radiative transitions from the ground vibrational level of the 1st excited electronic state to the ground state and the 1st excited vibrational levels of the ground electronic state of the porphyrin molecule.[38,39] The 420 nm wavelength was selected for FL excitation as it spectrally coincides with that of the most intensive B peak of the absorption spectrum of the ZnTPP molecule.

The dependence of absorption and fluorescence (FL) spectra of aqueous solutions of ZnTPP/D-*g*-PAA/AuNP and ZnTPP/D-*g*-PAA/AgNP triple nanohybrids on the polymer and gold/silver concentration was investigated (Fig. 4 and 5, respectively). For convenience of analyzing the transformation of absorption and FL spectra with increasing concentrations of D-*g*-PAA and metal, the spectra were normalized by intensity.

The absorption spectra (Fig. 4(a) and 5(a)) contain peaks of varying natures: (1) B and Q peaks of the ZnTPP molecule (denoted as ZnTPP: B and ZnTPP: Q, respectively); (2) peaks of light absorption by Au NPs (Au: LSPR – peak of localized surface plasmon resonance with a maximum at 525 nm and Au: interband – peak of interband transitions in gold) or Ag NPs (Ag: LSPR – peak of localized surface plasmon resonance with a maximum at 400 nm and Ag: interband – peak of interband transitions in silver); and (3) absorption peak of the polymer (D-*g*-PAA) at wavelengths shorter than 250 nm. The absorption spectra show that the addition of an ethanol solution of ZnTPP to an aqueous solution of the polymer–metal nanohybrid leads to the blurring of the doublet structure of the B peak likely due to the hydrophobic interaction of ZnTPP molecules with water. It is also evident that increasing the concentration of polymers and metals leads to an expected increase in the intensity of their absorption peaks.

The B peak of the ZnTPP molecule (420 nm) and the plasmonic LSPR peak of Ag NPs (400 nm) are spectrally resonant, while the LSPR peak of Au NPs (525 nm) is far from resonance with the B peak of ZnTPP. This suggests that the plasmon enhancement of electronic processes in ZnTPP molecules (particularly the photogeneration of ROS) in a nanohybrid containing Ag NPs should be much stronger than in one containing Au NPs. Additionally, it is well known that silver NPs generate a stronger plasmon field near their surfaces than gold NPs. Consequently, as described in Subsection "Cytotoxicity of nanohybrids to cancer cells", the activity of anticancer photodynamic therapy (PDT) of the ZnTPP/D-*g*-PAA/AgNP nanohybrid is significantly higher than that of the ZnTPP/D-*g*-PAA/AuNP variant.

In the vis range, the fluorescent centers of ZnTPP/D-*g*-PAA/AuNP and ZnTPP/D-*g*-PAA/AgNP nanohybrids are ZnTPP molecules, so the FL spectra of the nanohybrids (Fig. 4(b) and 5(b)) represent the FL spectrum of the ZnTPP molecule. However, it undergoes a transformation compared to the spectrum of ZnTPP in ethanol owing to the interaction of photosensitizer molecules with both the water and hybrid macromolecules of polymer/metal NPs. Fig. 4(a) and 5(a) show that an increase in the concentration of polymer and Au(Ag) leads to a significant transformation of the FL spectrum. First, there is a notable 2.7-fold decrease in the intensity of the short-wavelength F_{00} peak compared to the intensity of the long-wavelength F_{01} peak (at a concentration of 0.1952 mg per mL D-*g*-PAA/AuNPs and 0.0210 mg per mL D-*g*-PAA/AgNPs), which reflects changes in the probabilities of the corresponding radiative transitions in the ZnTPP molecule. Second, there is a 10 nm red shift of the more intense F_{01} peak at the same polymer and metal concentrations, indicating a change in the energy spectrum of the photosensitizer molecule. Moreover, with an increase in the concentration of the D-*g*-PAA/Au(Ag)NP nanohybrid, both

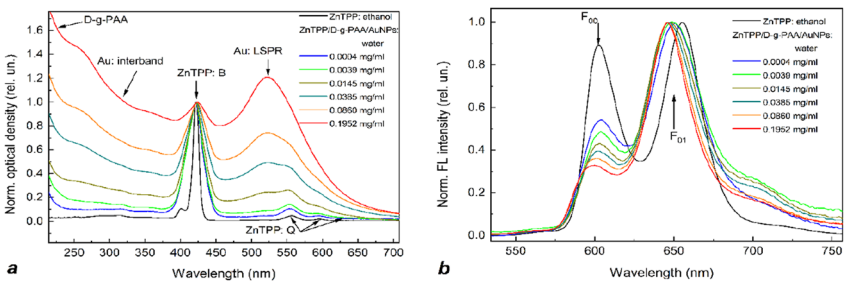

Fig. 4 Normalized absorption (a) and fluorescence (b) spectra of the ZnTPP/D-*g*-PAA/AuNP nanohybrid in water under different concentrations of D-*g*-PAA and Au. Spectra of ZnTPP in ethanol are given as reference. FL excitation wavelength: 420 nm. Concentrations: ZnTPP – 0.001 mg mL^{-1}, D-*g*-PAA and Au – in the range 0.0004–0.1952 mg mL^{-1}.

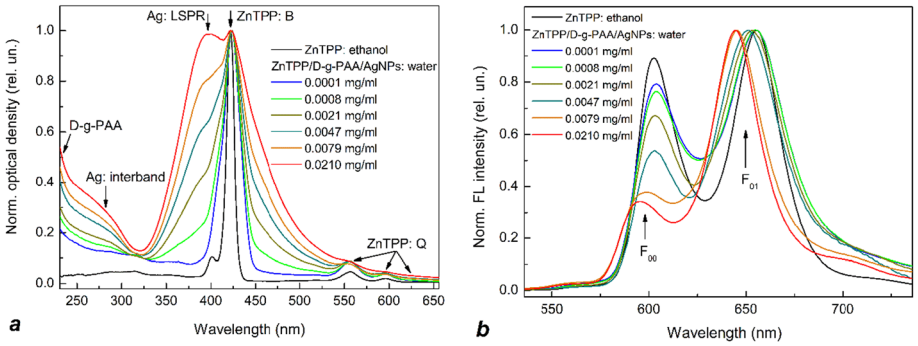

Fig. 5 Normalized absorption (a) and fluorescence (b) spectra of ZnTPP/D-*g*-PAA/AgNP nanohybrid in water under different concentrations of D-*g*-PAA and Ag. Spectra of ZnTPP in ethanol are given as a reference. FL excitation wavelength: 420 nm. Concentrations: ZnTPP – 0.001 mg mL^{-1}, D-*g*-PAA and Ag – in the range 0.0001–0.0210 mg mL^{-1}.

effects become stronger. These effects indicate the binding of ZnTPP molecules to hybrid macromolecules of both types: D-*g*-PAA/AuNPs and D-*g*-PAA/AgNPs.

Another evidence of the binding of ZnTPP molecules to D-*g*-PAA/Au(Ag)NP macromolecules is the results of FL anisotropy measurement, the method of which is described in Subsection "Optical spectroscopy" An increase in FL anisotropy should indicate a decrease in the number of degrees of freedom of the molecule as a result of its binding, in our case, to nanohybrids. It was found that the FL anisotropies of ZnTPP molecules in aqueous solutions of ZnTPP/D-*g*-PAA/AuNP and ZnTPP/D-*g*-PAA/AgNP nanohybrids are 0.24 and 0.18, respectively, indicating partial binding of photosensitizer molecules to hybrid macromolecules. Concurrently, ZnTPP molecules in ethanol are actually free, as evidenced by the FL anisotropy value of 0.07. Thus, the proven fact of binding of ZnTPP molecules to D-*g*-PAA/Au(Ag)NP nanohybrids indicates the possibility of using D-*g*-PAA polymer macromolecules as nanocarriers, and Au and Ag NPs as plasmon enhancers of ROS photogeneration.

Cytotoxicity of nanohybrids to cancer cells

Au NPs containing nanohybrids. The results of the cytotoxicity studies of the dextran–polyacrylamide (D–PAA) copolymer-based nanohybrids are presented in Fig. 6. The cytotoxicity studies of the bare D–PAA copolymer revealed a slight decrease in the number of LNCaP cells, up to 10% of the initial number. Adding the two-component D-*g*-PAA/AuNP nanohybrid (without ZnTPP photosensitizer) with concentrations of copolymer and gold of 0.172 mg mL^{-1} and 0.086 mg mL^{-1} to the cell suspension reduces the number of cancer cells by 53% and 31%, respectively. The three-component ZnTPP/D-*g*-PAA/AuNP nanohybrid with the same concentrations of gold and polymer and ZnTPP concentration of 0.001 mg mL^{-1} shows similar effects: 49% and 23%. The two-component ZnTPP/D-*g*-PAA nanohybrid (without AuNPs) was also cytotoxic (36%) at D–PAA and ZnTPP concentrations of 0.172 mg mL^{-1} and 0.001 mg mL^{-1}, respectively. ZnTPP (0.001 mg mL^{-1}) does not affect the number of cells when added to the incubation medium.

An important condition for the use of light in photodynamic therapy is its minimal impact on healthy tissues. Ultraviolet radiation has too high photon energy, which can activate

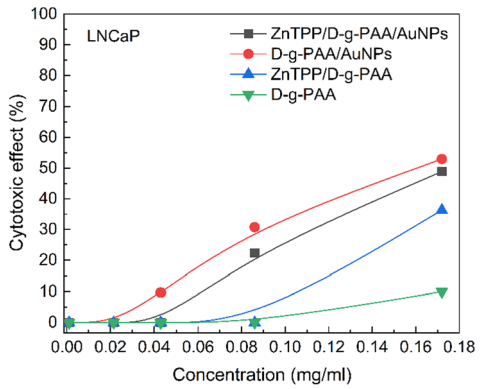

Fig. 6 Cytotoxicity of the ZnTPP/D-*g*-PAA/AuNP nanohybrid and its components on LNCaP prostate cancer cells. Concentrations: ZnTPP – 0.001 mg mL^{-1}, D-*g*-PAA/AuNPs and D-*g*-PAA were varied in the range 0.001–0.172 mg mL^{-1}.

mutagenesis and initiate cancerous transformation of cells.[51] The light of the blue range of the visible spectrum is less harmful but is still able to damage both photosensitive retinal cells and normal embryonic cells, causing oxidative stress.[52,53] Therefore, weak light power of 5, 10 and 20 mJ s^{-1} with total doses of 1, 2, 3 and 5 J cm^{-2} was chosen to study the phototoxicity of blue 420 nm light on LNCaP prostate cancer cells. A wavelength of 420 nm was used for irradiation because it coincides with the Soret absorption peak of the ZnTPP molecule. Initially, experiments were performed on LNCaP cells in an incubation solution. The obtained results are shown in Fig. 7. A weak phototoxicity of 420 nm light was revealed, which did not exceed 30% at irradiation doses of 2, 3, and 5 J cm^{-2} with light power of 10 and 20 mJ s^{-1}.

For further study of the phototoxic effect of the ZnTPP/D-*g*-PAA/AuNP nanohybrid and its individual components on LNCaP prostate cancer cells under 420 nm light irradiation, two irradiation parameters were chosen, namely doses of 1 J cm^{-2} and 2 J cm^{-2} with a light power of 10 mJ s^{-1}, which have a minimal effect on cells, and simultaneously, in our opinion, are sufficient for the initiation of ROS photogeneration by ZnTPP molecules. The concentration of AuNPs was 0.086 mg

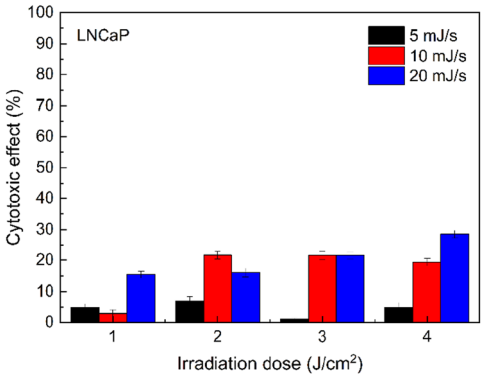

Fig. 7 Cytotoxicity of 420 nm light on LNCaP prostate cancer cells. Light power – 5, 10, and 20 mJ s^{-1}; irradiation dose – 1, 2, 3, and 5 J cm^{-2}.

mL^{-1}, providing stable cytotoxic effects against the prostate cancer cells of the LNCaP line. No statistically significant differences were found in the anticancer activity of the ZnTPP/D-*g*-PAA nanohybrid after irradiation with 420 nm light with a total dose of 1 J cm^{-2} (Fig. 8(a)).

The ZnTPP/D-*g*-PAA/AuNP triple nanohybrid combined with 420 nm light provides a 45% reduction in the LNCaP cell population, which is 15% higher than the photoinduced cytotoxicity of D-*g*-PAA/AuNPs double nanohybrid. Increasing the total irradiation dose to 2 J cm^{-2} almost does not change the efficiency of the triple nanohybrid, which is 47% (Fig. 8(b)). Therefore, the use of a 420 nm light of low power can increase the anticancer activity of the ZnTPP/D-*g*-PAA/AuNP nanohybrid, and increasing the dose promotes the appearance of phototoxic effects of light without significantly changing the anticancer activity of the nanohybrid. Thus, owing to the high cytotoxic activity of the D-*g*-PAA/AuNP nanohybrid combined with 420 nm light irradiation, it has a high potential for the photodynamic treatment of prostate cancer.

Ag NPs containing nanohybrids. The cytotoxic effect of D-*g*-PAA/AgNPs double nanohybrid was tested by applying the method of five-fold dilutions of the initial concentration of 0.14 mg mL^{-1} in the range of 0.023–0.0000368 mg mL^{-1} (Fig. 9). The addition of D-*g*-PAA/AgNPs nanohybrid to the suspension of LNCaP prostate cancer cells at concentrations of 0.023 mg mL^{-1} and 0.0047 mg mL^{-1} reduces the number of cancer cells by 83 and 52%, respectively. The ZnTPP/D-*g*-PAA/AgNP triple nanohybrid has a similar effect of 87 and 47% reduction at the same gold and polymer concentrations (Fig. 9).

The maximum absorption peak of the ZnTPP photosensitizer and the LSPR in AgNPs is approximately 420 nm.

Therefore, when the ZnTPP/D-*g*-PAA/AgNP triple nanohybrid is irradiated with such wavelength light, ROS generation by ZnTPP molecules and surface plasmon excitation in the Ag NPs occur. Under such conditions, with an irradiation dose of 1 J cm^{-2}, the cytotoxic effect of ZnTPP/D-*g*-PAA/AgNP nanohybrid is 83% (Fig. 10(a)). Without irradiation, the ZnTPP/D-*g*-PAA/AgNP nanohybrid reduces the number of cells by 47%. The concentration of Ag NPs used is 0.0047 mg mL^{-1}. Increasing the radiation dose to 2 J cm^{-2} leads to a slight decrease in the cytotoxicity to 70% (Fig. 10(b)).

Thus, it can be concluded that irradiation with 420 nm light has a significant cytotoxic effect on LNCaP prostate cancer cells owing to the generation of reactive oxygen species. Owing to the high cytotoxic activity of the D-*g*-PAA/AgNPs nanohybrid, it has a high potential for the treatment of prostate cancer. The main cytotoxic effects of silver NPs are

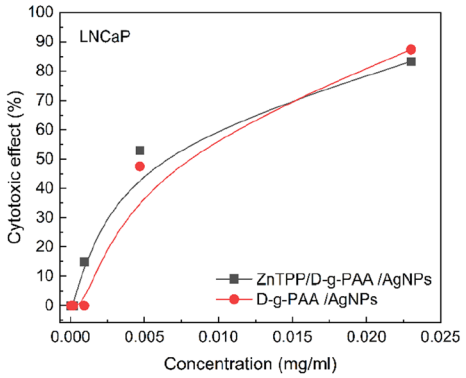

Fig. 9 Cytotoxicity of D-*g*-PAA/AgNPs on LNCaP prostate cancer cells. Concentrations: ZnTPP – 0.001 mg mL^{-1}, D-*g*-PAA and D-*g*-PAA/AgNPs was varied in the range 0.0023–0.0000368 mg mL^{-1}.

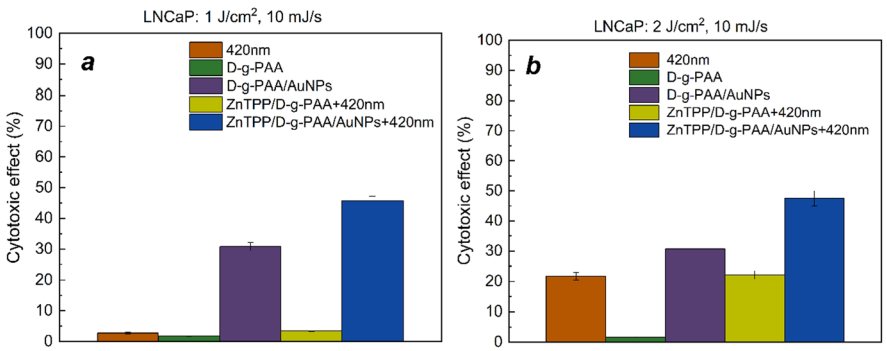

Fig. 8 Cytotoxicity of the ZnTPP/D-*g*-PAA/AuNP nanohybrid and its individual components on LNCaP prostate cancer cells under 420 nm light irradiation. Concentrations: ZnTPP – 0.001 mg mL^{-1}, D-*g*-PAA/AuNPs and D-*g*-PAA – 0.086 mg mL^{-1}, light power – 10 mJ s^{-1}, irradiation dose – 1 J cm^{-2} (a) and 2 J cm^{-2} (b).

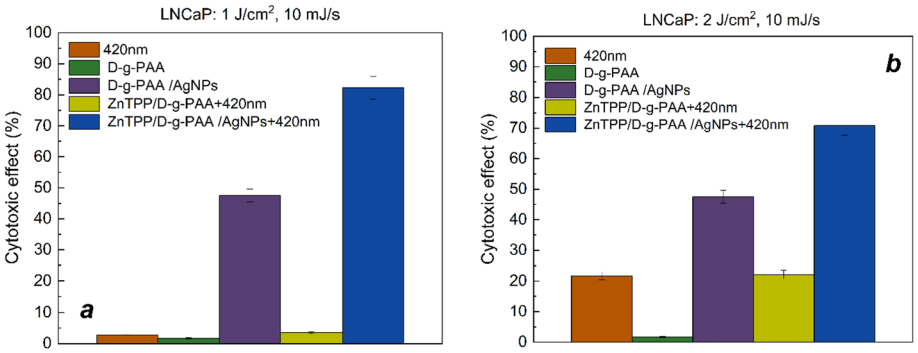

Fig. 10 Cytotoxicity of the ZnTPP/D-*g*-PAA/AgNP nanohybrid and its components on LNCaP prostate cancer cells under 420 nm light irradiation. Concentrations: ZnTPP – 0.001 mg mL^{-1}, D-*g*-PAA/AgNPs and D-*g*-PAA – 0.0047 mg mL^{-1}, light power – 10 mJ s^{-1}, irradiation dose – 1 J cm^{-2} (a) and 2 J cm^{-2} (b).

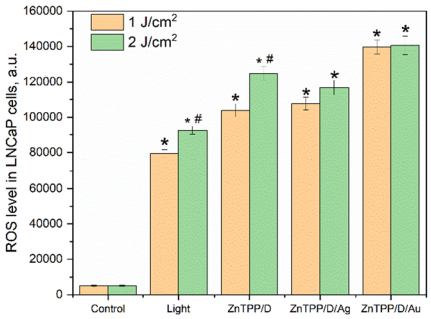

Fig. 11 Reactive oxygen species (ROS) level in LNCaP prostate cancer cells after treatment with ZnTPP/D-*g*-PAA (ZnTPP/D), ZnTPP/D-*g*-PAA/AgNPs (ZnTPP/D/Ag) and ZnTPP/D-*g*-PAA/AuNPs (ZnTPP/D/Au) under a light irradiation of 420 nm (light). Concentrations: ZnTPP – 0.001 mg mL^{-1}, D-*g*-PAA/AuNPs and D-*g*-PAA – 0.0047 mg mL^{-1}, D-*g*-PAA/AuNPs and D-*g*-PAA – 0.086 mg mL^{-1}, light power – 10 mJ s^{-1}, irradiation dose – 1 J cm^{-2} and 2 J cm^{-2}; (*p < 0.05 relative control, $^{\#}p$ < 0.05 relative irradiation dose 1 J cm^{-2}).

provided by the release of Ag^+ ions and their interaction with cell components. First, these are SH-groups located in the active centers of enzymes. Other interactions with membranes and nucleic acids are possible.[1]

ROS levels in cancer cells

The ROS level in cells was measured during the incubation of LNCaP prostate cancer cells with nanohybrids under 420 nm light irradiation (Fig. 11).

An increase in ROS by 15 times and 18 times from the initial level was found after cells were irradiated with 420 nm light at doses of 1 J cm^{-2} and 2 J cm^{-2}, respectively. ROS generation was enhanced during the incubation of the cells with ZnTPP/D-*g*-PAA. Dose-dependent changes in ROS were detected upon irradiation of untreated cells and after incubation with ZnTPP/D-*g*-PAA. AgNPs-containing nanohybrids did not change ROS generation in LNCaP cells relative to ZnTPP/D-*g*-PAA under 420 nm light irradiation. AuNPs-containing nanohybrids increased ROS generation compared to ZnTPP/D-*g*-PAA by 1.3 times and 27 times compared to the basic ROS level. Blue light is well absorbed by porphyrin and flavin structures.[54] Large doses of blue light irradiation promote cell damage. The results of ROS generation under 420 nm of light irradiation confirm this statement.

Conclusions

The 420 nm light irradiation of low power (10 mJ s^{-1}) has a significant cytotoxic effect on LNCaP prostate cancer cells *in vitro* by adding ZnTPP/D-*g*-PAA/AuNPs and ZnTPP/D-*g*-PAA/AgNPs hybrid nanohybrids into the incubation solution. Meanwhile, it is advisable to use low doses of irradiation (1 J cm^{-2}) because an increase in the dose promotes the phototoxic effects of light without a significant increase in anticancer activity. ZnTPP/D-*g*-PAA/AgNP nanohybrids have considerably higher anticancer activity (82%) compared to ZnTPP/D-*g*-PAA/AuNPs (45%). Most possibly, for ZnTPP/D-*g*-PAA/AgNP nanohybrid, it is due to resonance of light irradiation wavelength of 420 nm both with absorption Soret peak of the ZnTPP photosensitizer and LSPR in Ag NPs. Meanwhile, for ZnTPP/D-*g*-PAA/AuNP nanohybrid, the 420 nm light is out of resonance with LSPR in Au NPs. Therefore, the plasmon enhancement of ROS by ZnTPP molecules is considerably higher for the nanohybrid containing the Ag NPs compared to the one with Au NPs. Another possible cause of the higher anticancer activity of silver containing nanohybrids is the higher cytotoxicity of Ag NPs than Au NPs. AuNPs and AgNP nanohybrids increased ROS levels in LNCaP prostate cancer cells under 420 nm light irradiation of low power and irradiation dose. In conclusion, owing to the high cytotoxic activity of D-*g*-PAA/AgNPs and D-*g*-PAA/AuNP hybrid nanohybrids combined with low-power light irradiation at a wavelength of 420 nm, such nanohybrids have quite high potential in the photodynamic treatment of prostate cancer.

Author contributions

Conceptualisation (Oleg Yeshchenko, Nataliya Kutsevol), formal analysis (Pavlo Virych, Vasyl Chumachenko, Vasyl Cekhun), investigation (Oleg Yeshchenko, Petro Virych, Pavlo Khort, Vasyl Chumachenko, Pavlo Virych), methodology (Oleg Yeshchenko, Nataliya Kutsevol, Vasyl Cekhun), project

administration (Oleg Yeshchenko), validation (Oleg Yeshchenko, Pavlo Virych, Nataliya Kutsevol), writing – original draft (Oleg Yeshchenko), writing – review & editing (Oleg Yeshchenko, Pavlo Virych, Nataliya Kutsevol).

Conflicts of interest

There are no conflicts to declare.

Acknowledgements

This study was supported in part by the Ministry of the Education and Science of Ukraine, project no. 0122U00181 "Hybrid nanosystems based on "smart" polymers for biotechnology and medicine" and by National Research Foundation of Ukraine, project 2020.02/0022 "Plasmon hybrid nanosystems "metal–polymer–fluorophore" with enhanced optical response for photonics and biomedical applications". The authors thank French PAUSE program for emergency welcome of Ukrainian scientist Dr Nataliya Kutsevol in 2022–2023 at University of Strasbourg-Institute Charles Sadron (Strasbourg, France); Mélanie Legros from the characterization group and Dr Michel Rawiso (Institut Charles Sadron, Strasbourg, France) for size exclusion chromatography characterization of the star-like polymer. Authors are grateful to brave defenders of Ukraine for the opportunity to finalize this publication.

Notes and references

1 A.-G. Niculescu and A. M. Grumezescu, *Appl. Sci.*, 2021, **11**, 3626.
2 X. Li, J. F. Lovell, J. Yoon and X. Chen, *Nat. Rev. Clin. Oncol.*, 2020, **17**, 657–674.
3 G. Gunaydin, M. E. Gedik and S. Ayan, *Front. Chem.*, 2021, **9**, 686303.
4 S. Qin, Y. Xu, H. Li, H. Chen and Z. Yuan, *Biomater. Sci.*, 2022, **10**, 51–84.
5 H. Abrahamse and M. R. Hamblin, *Biochem. J.*, 2016, **473**, 347–364.
6 S. Kwiatkowski, B. Knap, D. Przystupski, J. Saczko, E. Kędzierska, K. Knap-Czop, J. Kotlińska, O. Michel, K. Kotowski and J. Kulbacka, *Biomed. Pharmacother.*, 2018, **106**, 1098–1107.
7 J. H. Correia, J. A. Rodrigues, S. Pimenta, T. Dong and Z. Yang, *Pharmaceutics*, 2021, **13**, 1332.
8 X. Li, S. Lee and J. Yoon, *Chem. Soc. Rev.*, 2018, **47**, 1174–1188.
9 T. Koczorowski, A. Glowacka-Sobotta, M. Michalak, D. T. Mlynarczyk, E. Güzel, T. Goslinski and L. Sobotta, *Appl. Sci.*, 2023, **13**, 3933.
10 P. M. Giri, A. Banerjee and B. Layek, *Cancers*, 2023, **15**, 2256.
11 W. Gu, Z. Hua, Z. Li, Z. Cai, W. Wang, K. Guo, F. Yuan, F. Gao and H. Chen, *Biomater. Sci.*, 2022, **10**, 216–226.
12 Z. Wang, X. Ren, D. Wang, L. Guan, X. Li, Y. Zhao, A. Liu, L. He, T. Wang, A. V. Zvyagin, B. Yang and Q. Lin, *Biomater. Sci.*, 2023, **11**, 1116–1136.
13 P. Zhang, Q. Wu, J. Yang, M. Hou, B. Zheng, J. Xu, Y. Chai, L. Xiong and C. Zhang, *Acta Biomater.*, 2022, **146**, 450–464.
14 Z. Yang, R. Shi, X. Liu, Q. Zhang, M. Chen, Y. Shen, A. Xie and M. Zhu, *ACS Mater. Lett.*, 2023, **5**, 2361–2368.
15 S. Zhang, X. Sun, Z. Wang, J. Sun, Z. He, B. Sun and C. Luo, *ACS Appl. Mater. Interfaces*, 2022, **14**, 38497–38505.
16 S. J. Cameron, F. Hosseinian and W. G. Willmore, *Int. J. Mol. Sci.*, 2018, **19**, 2030.
17 H. Yu, Y. Peng, Y. Yang and Z. Y. Li, *npj Comput. Mater.*, 2019, **5**, 45.
18 J. J. Baumberg, J. Aizpurua, M. H. Mikkelsen and D. R. Smith, *Nat. Mater.*, 2019, **18**, 668–678.
19 W. Hou and S. B. Cronin, A review of surface plasmon resonance-enhanced photocatalysis, *Adv. Funct. Mater.*, 2013, **23**, 1612–1619.
20 Y. Zhang, K. Aslan, M. J. R. Previte and C. D. Geddes, *J. Fluoresc.*, 2007, **17**, 345–349.
21 A. Gandhi, A. Paul, S. O. Sen and K. K. Sen, *Asian J. Pharm. Sci.*, 2015, **10**, 99–107.
22 N. Macia, V. Kabanov, M. Côté-Cyr and B. Heyne, *J. Phys. Chem. Lett.*, 2019, **10**, 3654–3660.
23 N. Macia, V. Kabanov and B. Heyne, *J. Phys. Chem. C*, 2020, **124**, 3768–3777.
24 O. Planas, N. Macia, M. Agut, S. Nonell and B. Heyne, *J. Am. Chem. Soc.*, 2016, **138**, 2762–2768.
25 M. T. Yaraki, S. D. Rezaei and Y. N. Tan, *Phys. Chem. Chem. Phys.*, 2020, **22**, 5673–5687.
26 J. Peng and X. Liang, *Medicine*, 2019, **98**, 15311.
27 A. M. López-Marzo, R. Hoyos-de-la-Torrean and E. Baldrich, *Anal. Chem.*, 2018, **90**, 4010–4018.
28 A. El-Hussein and M. R. Hamblin, *IET Nanobiotechnol.*, 2017, **11**, 173–178.
29 A. Karabasz, M. Bzowska and K. Szczepanowicz, *Int. J. Nanomed.*, 2020, **15**, 8673–8696.
30 N. V. Kutsevol, V. A. Chumachenko, I. I. Harahuts and A. I. Marinin, in *Chemical Engineering of Polymers. Production of Functional and Flexible Materials*, ed. O. V. Mukbanianym, M. J. Abadie and T. Tatrishvili, Apple Academic Press, 2017, pp. 119–129.
31 D. L. Hao, R. Xie, G. J. De, H. Yi, C. Zang, M. Y. Yang, L. Liu, H. Ma, W. Y. Cai, Q. H. Zhao, F. Sui and Y. J. Chen, *Int. J. Nanomed.*, 2020, **15**, 1771–1786.
32 Y. Jiang, Y. Zhou, C. Y. Zhang and T. Fang, *Int. J. Nanomed.*, 2020, **15**, 3319–3331.
33 Q. Zhou, L. Zhang, T. Yang and H. Wu, *Int. J. Nanomed.*, 2018, **13**, 2921–2942.
34 N. K. Preman, R. R. Barki, A. Vijayan, S. G. Sanjeeva and R. P. Johnson, *Eur. J. Pharm. Biopharm.*, 2020, **157**, 121–153.
35 F. Farjadian, S. Rezaeifard, M. Naeimi, S. Ghasemi, S. Mohammadi-Samani, M. E. Welland and L. Tayebi, *Int. J. Nanomed.*, 2019, **14**, 6901–6915.
36 V. A. Chumachenko, I. O. Shton, E. D. Shishko, N. V. Kutsevol, A. I. Marinin and N. F. Gamaleia, in *Nanophysics, Nanophotonics, Surface Studies, and Applications, Springer Proceedings in Physics Series*, ed. O. Fesenko and L. Yatsenko, Springer, Cham, Switzerland, 2016, vol. 183, pp. 379–390.

37 A. M. De Pinillos Bayona, P. Mroz, C. Thunshelle and M. R. Hamblin, *Chem. Biol. Drug Des.*, 2017, **89**, 192–206.
38 J. Elms, P. N. Beckett, P. Griffin and A. D. Curran, *Toxicol. In Vitro*, 2001, **15**, 631.
39 O. A. Yeshchenko, N. V. Kutsevol, A. V. Tomchuk, P. S. Khort, P. A. Virych, V. A. Chumachenko, Y. I. Kuziv, A. P. Naumenko and A. I. Marinin, *RSC Adv.*, 2022, **12**, 11.
40 O. A. Yeshchenko, N. V. Kutsevol, A. V. Tomchuk, P. S. Khort, P. A. Virych, V. A. Chumachenko, Y. I. Kuziv, A. I. Marinin, L. Cheng and G. Nie, *Nanomaterials*, 2022, **12**, 2655.
41 O. A. Yeshchenko, N. V. Kutsevol, A. V. Tomchuk, P. S. Khort, P. A. Virych, V. A. Chumachenko, Y. I. Kuziv, A. P. Naumenko and A. I. Marinin, *Nanomed. Res. J.*, 2022, **7**, 173.
42 N. Kutsevol, T. Bezugla, M. Bezuglyi and M. Rawiso, *Macromol. Symp.*, 2012, **317–318**, 82–90.
43 N. Kutsevol, Yu. Kuziv, T. Bezugla, P. Virych, A. Marynin, T. Borikun, N. Lukianova, P. Virych, V. Chekhun and N. Kutsevol, *Appl. Nanosci.*, 2022, **12**, 427–437.
44 T. Matvienko, V. Sokolova, S. Prylutska, Y. Harahuts, N. Kutsevol, V. Kostjukov, M. Evstigneev, Y. Prylutskyy, M. Epple and U. Ritter, *Bioimpacts*, 2019, **9**, 57–63.
45 X. Yuan, Z. Liu, Y. Wang, Y. Xu, W. Zhang and T. Mu, *J. Quant. Spectrosc. Radiat. Transf.*, 2020, **246**, 106917.
46 B. R. Nayak and R. P. Singh, *Eur. Polym. J.*, 2001, **37**, 1655.
47 D. F. Marsh and L. M. Mink, *J. Chem. Educ.*, 1996, **73**, 1181.
48 J. P. Strachan, S. Gentemann, J. Seth, W. A. Kalsbeck, J. S. Lindsey, D. Holten and D. F. Bocian, *J. Am. Chem. Soc.*, 1997, **119**, 11191–11201.
49 A. Harriman, *J. Chem. Soc., Faraday Trans. 1*, 1980, **76**, 1978–1985.
50 K. A. Nguyen, P. N. Day, R. Pachter, S. Tretiak, V. Chernyak and S. Mukamel, *J. Phys. Chem. A*, 2002, **106**, 10285–10293.
51 M. Watson, D. M. Holman and M. Maguire-Eisen, *Semin. Oncol. Nurs.*, 2016, **32**, 241–254.
52 K. Ratnayake, J. L. Payton, M. E. Meger, N. H. Godage, E. Gionfriddo and A. Karunarathne, *Cell. Signal.*, 2020, **69**, 109547.
53 A. C. Wall, J. P. Gius, D. J. Buglewicz, A. B. Banks and T. A. Kato, *Mutat. Res. Genet. Toxicol. Environ. Mutagen*, 2019, **841**, 31–35.
54 J. X. Tao, W. C. Zhou and X. G. Zhu, *Oxid. Med. Cell. Longev.*, 2019, **2019**, 6435364.